THE AMERICAN SOCIETY OF MECHANICAL ENGINEERS
345 E. 47th St., New York, N.Y. 10017

97-GT-86

Reduction of Unsteady Blade Loading by Beneficial Use of Vortical and Potential Disturbances in an Axial Compressor with Rotor Clocking

S.T. Hsu[1] and Andrew M. Wo[2]

Institute of Applied Mechanics
National Taiwan University
Taipei 106, Taiwan, R.O.C

ABSTRACT

This paper demonstrates reduction of stator unsteady loading due to forced response in a large-scale, low-speed, rotor/stator/rotor axial compressor rig by clocking the downstream rotor. Data from the *rotor/stator* configuration showed that the stator response due to the upstream vortical disturbance reaches a *maximum* when the wake impinges against the suction surface immediately downstream of the leading edge. Results from the *stator/rotor* configuration revealed that the stator response due to the downstream potential disturbance reaches a *minimum* with a slight time delay after the rotor sweeps pass the stator trailing edge. For the *rotor/stator/rotor* configuration, with Gap1= 10% chord and Gap2= 30% chord, results showed a 60% reduction in the stator force amplitude by clocking the downstream rotor so that the time occurrence of the maximum force due to the upstream vortical disturbance coincides with that of the minimum force due to the downstream potential disturbance. This is the first time, the authors believe, that beneficial use of flow unsteadiness is definitively demonstrated to reduce the blade unsteady loading.

1.0 INTRODUCTION

Multi-stage turbomachinery blades experience fluid-induced, unsteady force either due to self-excited instability or forced response. The first situation arises when a blade is able to extract energy from the upstream *steady* flow in order to sustain its own unsteady motion. The latter case involves flow disturbances, or gust, which usually arise due to the passing of upstream wakes, potential effect from upstream and downstream blade rows, and other time varying local flows. In both situations, disastrous blade failure can occur when the excitation force is beyond the structural limit of the blade.

Forced response had been studied by many researchers. Theoretical work on unsteady disturbances includes Goldstein and Atassi (1976) and Goldstein (1978). Excellent series of experiments (Henderson and Fleeter, 1993a & 1993b; Feiereisen et al., 1993; Weaver and Fleeter, 1994) were conducted by Professor Fleeter and his students on illuminating the physics of vortical and potential disturbances. Gallus et al. (1982) also studied potential and wake interactions experimentally. The work by Manwaring and Wisler (1993) provided extensive comparison between the state-of-the-art analysis methods and data. Chung and Wo (1995) used both Navier-Stokes and panel codes to split the gust between blade rows into vortical and potential contributions, and Wo et al. (1997) provided details on decomposition of gust response. Although the researchers aforementioned differ somewhat in their approach to decompose disturbances into vortical and potential contributions all agree that both need to be considered for loaded compressors and turbines, especially at small axial gap.

Clocking, or indexing, of blade rows had been conducted in a few studies. Capece and Fleeter (1987) circumferentially clocked the first and second stator rows independently to study their effects on aerodynamic forcing function input to the downstream stator row, and its gust response. This form of clocking mostly affected the chordwise gust of the aerodynamic function, with a small effect on the overall blade unsteady loading, since the clocked stators upstream were in the same reference frame as the downstream stator of interest. Manwaring and Wisler (1993) clocked both the IGV of the GE

1 Doctoral Student

2 Associate Professor (E-mail: andrew@spring.iam.ntu.edu.tw)

Presented at the International Gas Turbine & Aeroengine Congress & Exhibition
Orlando, Florida — June 2–June 5, 1997
This paper has been accepted for publication in the Transactions of the ASME
Discussion of it will be accepted at ASME Headquarters until September 30, 1997

compressor and the inlet nozzle of the turbine in order to average the effect of their wakes on the instrumented stationary blades downstream. The authors believe that the present study is the first that documented concrete reduction of unsteady blade loading using clocking.

2.0 OBJECTIVE AND APPROACH

This paper attempts to test a straightforward hypothesis – distinct physical sources of disturbance will cause an unique "footprint" on the unsteady blade response, and these "footprints" may partially cancel each other if, somehow, their phase relationship can be altered. This hypothesis will be tested experimentally for a rotor/stator/rotor compressor with the focus on the stator unsteady response. Sources of unsteadiness experience by the stator include[1]

1. vortical disturbance from the *upstream* rotor (R1),
2. potential disturbance from the *upstream* rotor and
3. potential disturbance from the *downstream* rotor (R2).

These are shown in Fig. 1, calculated using a Navier-Stokes code (Chung and Wo, 1995).

To test the hypothesis and to provide physical insight the following approach is taken. First, a *rotor/stator* configuration is tested to study the first two sources of unsteadiness. The axial gap between the rotor and stator is varied since the gap can affect the stator response due to the potential contribution. Second, a *stator/rotor* configuration is studied to focus on the third source of unsteadiness considered. Third, a *rotor/stator/rotor* configuration is tested to account for all three sources. The circumferential relative position between the two rotor rows are adjusted, or *clocked*, to vary the phase relationship among the unsteady sources, with the ultimate goal of minimizing the stator unsteady response. This goal is justified since a small percentage reduction in the blade force amplitude can lead to a substantial increase in blade life, as suggested by the blade stress-cycle, or Goodmann, diagram.

3.0 EXPERIMENTAL SETUP

The experimental compressor is a low-speed, large-scale, one-to-three stage rig, designed after modern compressors, see Table 1 and Fig. 2. Flow enters the compressor through a bell-mouth contraction and into the constant blade height annulus. The IGV trailing edge is located 1.75 chord upstream of the rotor leading edge to allow for wake dissipation. The blades were designed using controlled diffusion concept of Hobbs and Weingold (1984), with the coordinates provided in the Appendix. Two special features are designed in the rig: axial gaps between blade rows are variable, from 10% to 60% chord, and the clocking position between rotor rows can be adjusted.

The measured static-to-static pressure rise characteristic is shown in Fig. 3. The pressure rise obtained is believed to be representative of highly loaded blade of modern design. In this

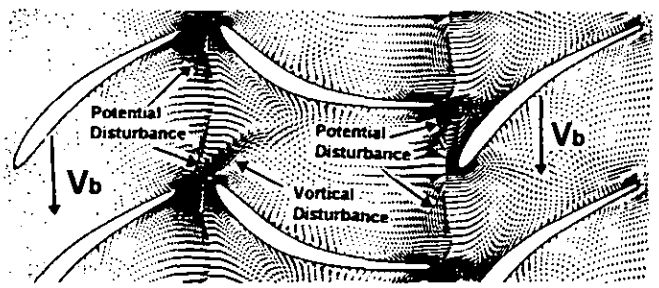

Fig. 1 Sources of disturbance acting on the stator: vortical and potential disturbances from upstream and potential disturbance from downstream (Navier-Stokes calculation).

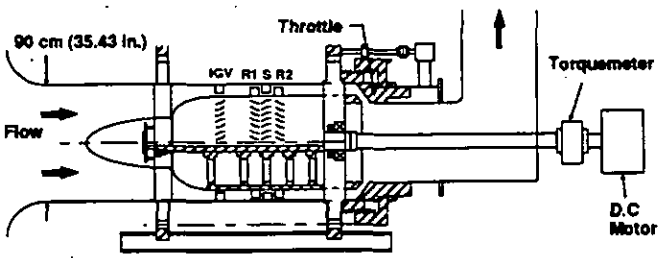

Fig. 2 Experimental compressor in the rotor/stator/rotor configuration.

Nomenclature

C	chord
F_n	force on the stator, normal to chord
P	static pressure
S	blade pitch
t, T	time, blade-to-blade period
$\mathbf{V}_b$	rotor blade wheel velocity vector
v^+	transverse component of unsteady velocity
ρ	density of fluid
Φ	flow coefficient
C_x	axial velocity
ΔP_s	static pressure rise

Headed Quantities

$\overline{\quad}$	time mean
$\sim$	unsteady part, instantaneous minus time mean

[1] To address the issue of the importance of entropic disturbance raised by a reviewer, consider the linearized disturbance $Ds' / Dt = (Cv / P_0)\, Dp' / Dt - (Cp / \rho_0)\, Dp' / Dt$ (Kerrebrock, 1992), where the subscript 0 denotes the mean state and the superscript ' denotes disturbed state. In the experiment the change in the particle density term can be ignored since the stator inlet Mach number is 0.113. An order of magnitude calculation shows the entropic disturbance is less than 1% of the pressure disturbance.

work, tests were conducted at near-design loading (Φ= 0.60) and high loading (Φ= 0.53). The compressor achieves an efficiency, based on static-to-static pressure rise, of slightly over 90% for rotor/stator configuration at both 10% and 30% chord axial gaps.

In this work, three compressor configurations were tested: rotor/stator, stator/rotor and rotor/stator/rotor, as sketched in Figs. 4, 5 and 6, respectively. In all these figures, the dash lines defined the blade relative position at time t/T= 0.0 in an unsteady period. Figure 4 shows the definition of *positive* stator unsteady force normal to the chord, which is used throughout this work for all configurations. In the stator/rotor configuration, a row of upstream rotors, with its trailing edge located two chord-length upstream of the stator leading edge, provided correct flow angles entering the stators. To establish the baseline for this arrangement, tests were conducted with the upstream rotors and the stators but without the downstream rotors. The gust at the stator leading edge plane was measured to be less than 2% of the time mean flow, and the stator response was also measured, which was subtracted from all stator/rotor data reported herein. For the rotor/stator/rotor configuration, Fig. 6 serves to define the *clocking* between Rotor 1 and Rotor 2, which is the distance that the leading edge of Rotor 2 is offset circumferentially from

	IGV	Rotor (R1 or R2)	Stator
Blade Number	60	58	60
Chord (cm), C	6.00 (2.36in.)	6.00 (2.36in.)	6.00 (2.36in.)
Span (cm), S	8.88 (3.50in.)	8.88 (3.50in.)	8.88 (3.50in.)
Solidity	1.415	1.368	1.415
Tip Clearance (cm)	0.12 (2.0%C)	0.12 (2.0%C)	0.12 (2.0%C)
Aspect Ratio (S/C)	1.48	1.48	1.48
Trailing Edge Radius	1.0 %C	1.0 %C	1.0 %C
Stagger (deg.)	6.58°	-39.50°	20.67°
Camber (deg.)	3.2°	35.0°	48.0°
Inlet Angle, β 1 (deg.)*	0.0°	56.21°	46.80°
Exit Angle, β 2 (deg.)*	9.78°	31.03°	4.76°
Diffusion Factor	-	0.407	0.485
Axial Gap (% chord)	175%	variable; see text	
Casing Diameter (cm)		90.0 (35.43 in.)	
Hub/Tip Ratio		0.8	
Mass Flow Coefficient		0.53 to 0.70	
Shaft Speed (RPM)		1050 (max. 1500)	
Reduced Frequency ($\omega C/2C_x$)		7.161	
Mach number (C_x/a)		0.0776	
Reynold's Number at 1050RPM (rotor relative)		1.92×10^5	

* from hot-wire at mid-gap, mid-pitch, for axial gap of 30% chord.

Table 1 General compressor and blade parameters at design condition.

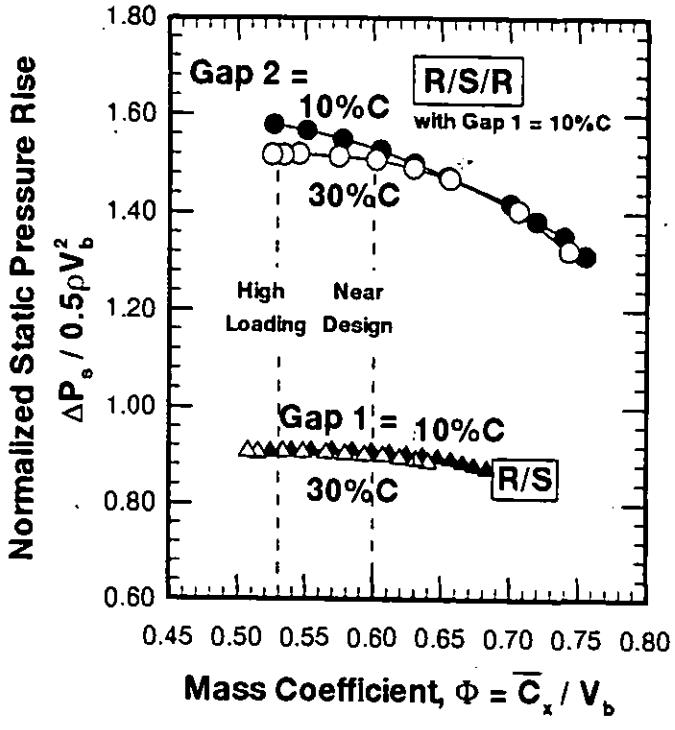

Fig. 3 Measured static-to-static pressure rise characteristic for rotor/stator and rotor/stator/rotor configurations with varying axial gaps.

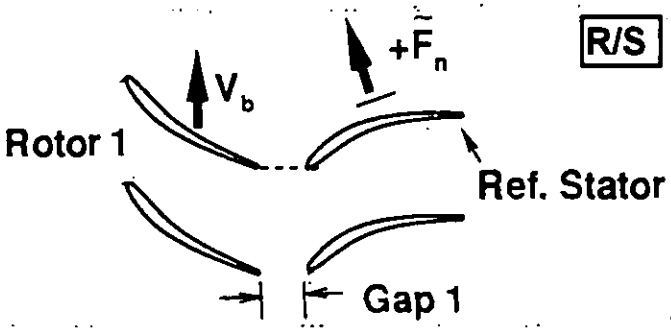

Fig. 4 Rotor/stator configuration at time t/T= 0.0; rotor trailing edge is axially upstream of the stator leading edge. Direction of *positive* stator force, normal to chord, is also shown.

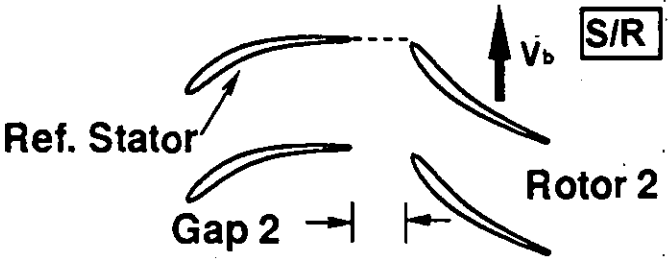

Fig. 5 Stator/rotor configuration at time t/T= 0.0; rotor leading edge is axially downstream of the stator trailing edge.

the stator trailing edge when the Rotor 1 trailing edge is axially upstream of the stator leading edge. In the compressor rig, the hub was designed in three cylindrical pieces, each can mount a row of rotor blades (thus the rig can be tested as a three-stage compressor), with the two downstream pieces movable circumferentially up to one blade pitch with respect to the adjacent piece.

The unsteady pressure on the stator suction and pressure surfaces were measured using fast-response pressure transducers (Kulite LQ-125), which were embedded within two adjacent blades (10 transducers per surface). The system response, calculated from Doebelin (1990), was found to be determined by the isolated transducer alone. Transducer signal of 128 data points in a rotor blade-to-blade period were acquired per shaft revolution, thus data from the *same* rotor wake were recorded. The pressure transducer output, as a differential signal, was connected to a low-noise amplifier (Stanford Research SR560), then digitized with a 12-bit analog-to-digital resolution. The accuracy of the surface pressure measurement is +/- 3% determined from calibration.

To provide timing information, a photo-sensitive diode was used to sense the passing of a metal protrusion rotating with the shaft, with a timing accuracy of 0.1% of a blade-to-blade period. To preserve the time series, an analog filter was not used prior to digitization, but the signal was monitored using a spectrum analyzer (HP 3561A) – no high frequency content exists which could aliase the blade-to-blade frequency and next few higher modes. Moreover, phase-locked averaging technique was also used to filter non-blade-to-blade periodic signals (240 typical ensembles were used).

Hsu et al. (1996) provides details on gust measurement using the slanted hot-wire technique, with an accuracy from calibration of +/- 1% in magnitude and +/- 1.5 degree in flow angles.

4.0 ROTOR/STATOR RESULTS: VORTICAL AND POTENTIAL DISTURBANCES FROM UPSTREAM OF STATOR

The rotor/stator configuration includes the effect of (a) rotor wake impinging upon the stator and subsequent wake convection along the stator passage and (b) the potential field of the rotor on the stator. Results due to these two phenomena follow for two axial gaps, Gap1= 10% and 30% chord.

4.1 Vortical and Potential Disturbances

Figure 7 presents the transverse vortical and potential gusts decomposed from slanted hot-wire data using the procedure described in Hsu et al. (1996) (also see Chung and Wo (1995), which used Navier-Stokes results where Hsu et al. used experimental data). The hot-wire was located axially upstream of the stator leading edge at the mid-gap position for both 10% and 30% chord gap cases.

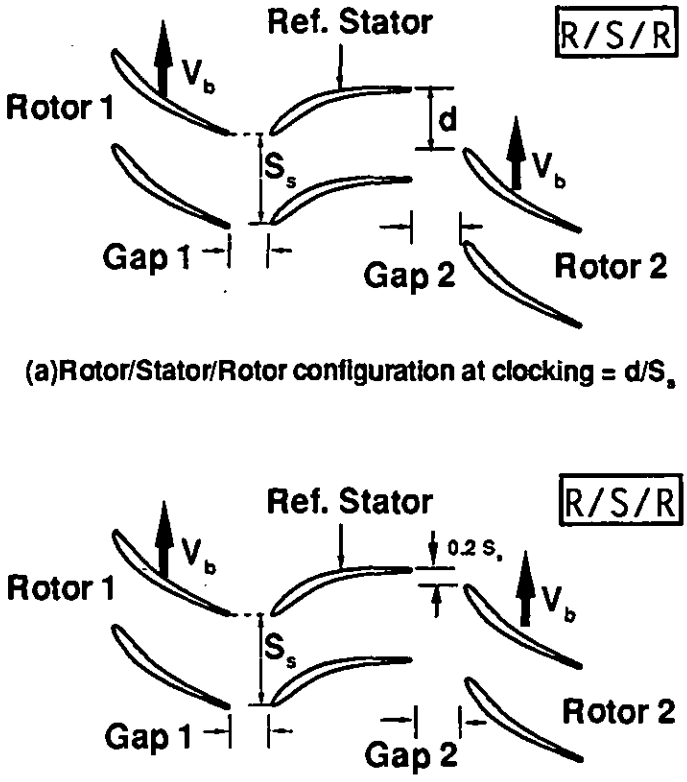

Fig. 6 Rotor/stator/rotor configuration at time t/T= 0.0 with downstream rotor clocked by d/Ss. Figure (a) shows clocking = 0.7 and (b) clocking = 0.2.

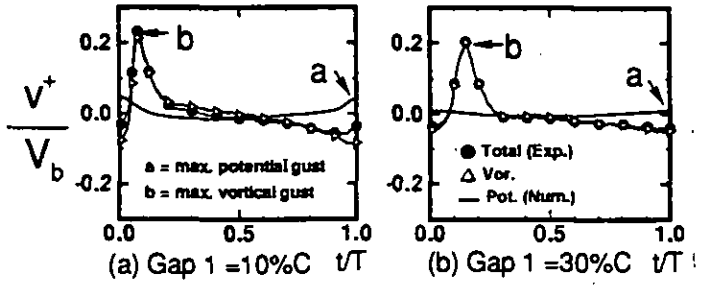

Fig. 7 Vortical and potential transverse gusts at the mid-gap point axially upstream of the stator leading edge (R/S).

The vortical gust signature shows an abrupt increase as the wake passes, which is the dominant feature for both gap cases. The vortical contribution essentially represents the total (prior to decomposition) transverse gust, since the potential contribution is small even at 10% chord gap between blade rows. Figure 7 thus provides further justification for using wake/blade calculation to model the unsteady effect from the upstream blade on the downstream blade (e.g., Giles, 1988 and Hall and Crawley, 1989). Moreover, the distinct difference in time scale between the vortical and potential gusts – the

vortical gust on the order of passing of the wake width and the potential gust being blade-to-blade period – can be clearly seen.

In this work, it is important to note the time when the gust reaches a maximum since phase information is vital to test the hypothesis stated in Section 2.0. Location 'a' represents the maximum value of the potential gust which occurs at t/T= 1.0, or 0.0 – this coincides with the time instant when the rotor trailing edge is axially forward of the stator leading edge, as shown in Fig. 4. The location marked 'b' represents the instant when the vortical gust is largest, which occurs at the time when the wake passes the hot-wire. Thus, the maximum vortical gust occurs when the rotor wake passes and the maximum potential gust occurs when the rotor blade itself passes. The reason that the time occurrence of location 'a' precedes that of 'b' is due to the rotor exit flow angle.

4.2 Stator Unsteady Loading

Figure 8 shows the near-design stator unsteady pressure on the suction and pressure surfaces for several time instants of interest. As can be seen spatial pressure variation is generally greater on the suction than that on the pressure surface, with a strong spike near the leading edge on the suction surface. This is due to the rotor wake impinges near the stator leading edge region, as confirmed by the time occurrence of maximum vortical gust (Fig. 7) essentially coincides with that of the pressure spike. The pressure spike occurs near t/T= 0.2 for 10% chord gap and t/T= 0.4 for 30% chord gap, which agree well with the wake impinges near the leading edge at t/T= 0.16* for 10% chord gap and t/T= 0.32* for 30% chord gap. The slight time delay between the pressure spike and the wake impingement suggests the response reaches a maximum when the wake arrives on the suction surface just downstream of the leading edge.

Secondary in importance is the pressure variation along the surface, as seen most prominently in Fig. 8a. Navier-Stokes calculation, which provides greater flow details within the stator passage, suggests that this is related to the wake requiring two blade-to-blade periods to convect through the stator passage on the suction surface. Numerics show that at time t/T= 0.3 the wakes are located near the leading edge and at x/C= 0.6 on the suction surface. Vorticity contour results suggest there is a region of concentrated vorticity adjacent to the suction surface at x/C= 0.6, which corresponds to the pressure variation near x/C= 0.6 in Fig. 8a. This is likely related to the work of Valkov and Tan (1995) which provides insight into the convection of, so-called, "B-vortices" on the suction surface. These vortices are formed upon wake

*This value is twice that corresponds to the maximum vortical gust in Fig. 7 since the data of Fig. 7 were obtained with the hot-wire located at the mid-gap position.

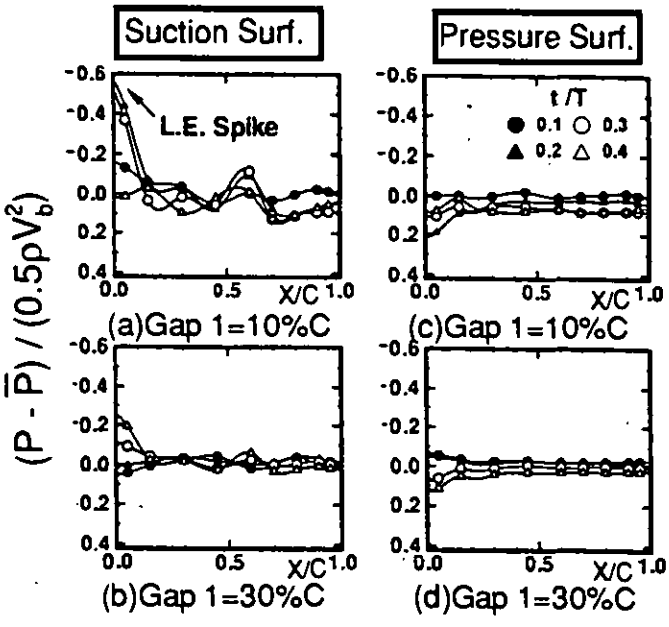

Fig. 8 Unsteady pressure on the stator surfaces with varying axial gap (R/S).

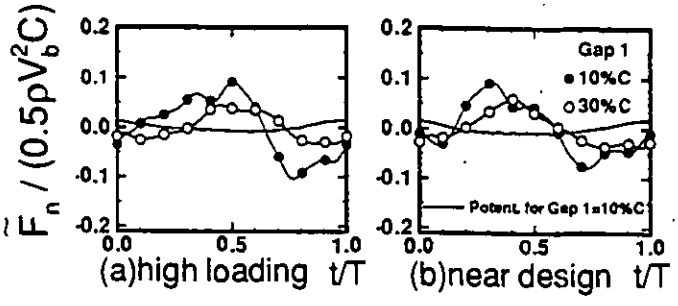

Fig. 9 Unsteady force on stator due to total and potential contributions with varying axial gap (R/S).

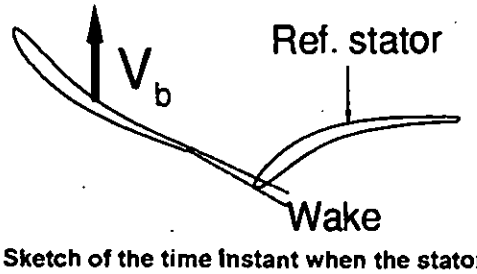

Fig. 10 Sketch of the time instant when the stator force reaches maximum (R/S).

impingement on the leading edge and move along the suction surface, which resulted in local pressure variation.

Figure 9 shows the stator unsteady force, in the direction normal to the chord, obtained by integrating the

unsteady pressure of Fig. 8. Results are shown for the total force, from surface Kulite output, and the potential contribution. The near-design loading result shows that the maximum unsteady force occurs at t/T= 0.3 for 10% chord gap and t/T= 0.4 at 30% chord gap. These times are in reasonable agreement with that of the pressure spike (t/T= 0.2 for 10% chord gap and t/T= 0.4 for 30% chord gap) of Fig. 8. Thus the maximum stator force occurs when the upstream wake impinges on the stator suction surface immediately downstream of the leading edge, as illustrated in Fig. 10.

The potential contribution in Fig. 8 is shown to be small even for 10% chord gap between blade rows. Thus the total force in Fig. 9 is almost entirely due to vortical contribution. This fact greatly simplifies testing of the hypothesis for rotor/stator/rotor configuration since the balance between unsteady forces on the stator is then between the vortical contribution from the upstream rotor wake and the potential contribution from the downstream rotor.

5.0 STATOR/ROTOR RESULTS: POTENTIAL DISTURBANCE FROM STATOR DOWNSTREAM

For the stator/rotor configuration, the stator experiences a gust response originated from the moving pressure field of the downstream rotor, if the axial gap between blade rows is not too large. Thus, this response is purely potential in nature; other sources of disturbance, e.g. the rotor wake, is small in comparison.

5.1 Stator Unsteady Loading

Figure 11 presents the stator suction surface unsteady pressure distribution at four consecutive time instants when the rotor leading edge sweeps pass the stator trailing edge. For Gap2= 10% chord, the time variation near the trailing edge suggests the stator begins to respond to the rotor passage near t/T= 0.0 to 0.1. (Recall that t/T= 0.0 is when the rotor leading edge is axially downstream of the stator trailing edge, see Fig. 5.) At t/T= 0.2 and 0.3, large suction spikes can be clearly seen. This feature is also present for Gap2= 30% chord but to a lesser degree. Data show that the time variation near the leading edge is much smaller than that at the trailing edge, which agrees with the understanding that potential disturbance decays exponentially, as shown by Chung and Wo (1995) and others. The unsteady pressure distribution on the stator pressure surface exhibits similar overall trend with approximately half the pressure amplitude of that on the suction surface.

Figure 12 shows the stator unsteady force normal to the chord. Data show a clear maximum and minimum in the signature, with the amplitude decreases with increased axial gap. This is certainly expected since the only unsteady source, the rotor downstream, is further separated from the stator. As before, the time instant when the force signature reaches an

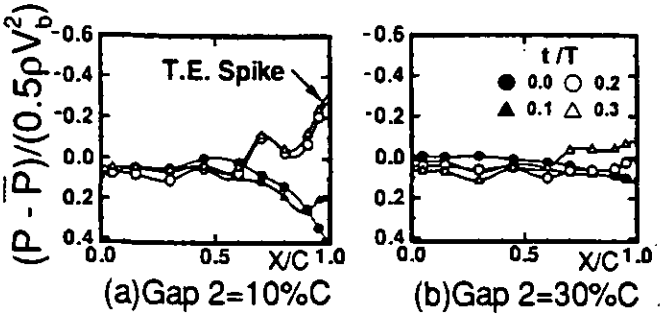

Fig. 11 Unsteady pressure on stator suction surface when the downstream rotor passes (S/R).

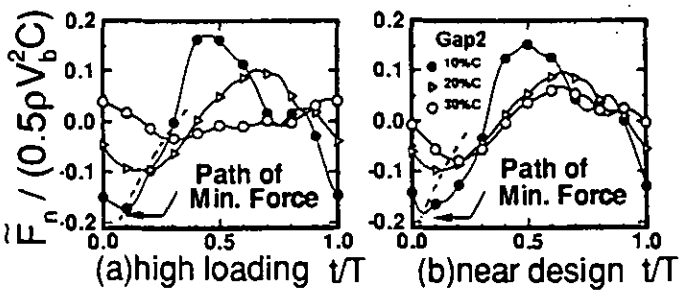

Fig. 12 Unsteady force on stator due to downstream potential disturbance with varying axial gap (S/R).

extremum is of primary interest. In the case of stator/rotor, the *minimum* in the force excursion is of concern since this is needed to, hopefully, offset the maximum in the rotor/stator configuration to reduce the unsteady loading for the rotor/stator/rotor configuration. At Gap2= 10% chord and near-design condition, Fig. 12b shows the unsteady force reaches a minimum near t/T= 0.05, which is *prior to* the occurrence of large pressure spike near the stator trailing edge as the rotor passes (see Fig. 11a). In other words, minimum force on the stator (defined in Fig. 4) is reached shortly after the rotor leading edge passes the stator trailing edge. This time lag increases with increasing axial gap, as shown by the path of minimum force in Fig. 12. Figure 12b shows the force minimum is delayed to t/T= 0.2 for an axial gap of 30% chord, along with a decrease in the amplitude.

5.2 Potential Disturbances from Upstream and Downstream

Results thus far show a curious fact that the extent of the effect of potential disturbance differ greatly between rotor/stator and stator/rotor configurations. Figure 13 presents the potential induced unsteady force on the stator for the two configurations, with axial gaps of 10% and 30% chord for both cases. (The rotor/stator results are taken from Fig. 9 and the stator/rotor from Fig. 12.) Results suggest that the unsteady force response contributed by downstream potential disturbance

is substantially larger than that contributed by upstream potential disturbance for the same axial gap. At 30% chord gap, the effect of upstream disturbance is essentially zero while the downstream effect is clearly shown. The implication of this result for multi-stage compressors, where the rolor response is of primary interest, is that the axial gap between a stator and the downstream rotor can be smaller than that between the rotor and the successive stator, from the standpoint of potential disturbance alone.

6.0 ROTOR/STATOR/ROTOR RESULTS: WITH ALL THREE SOURCES OF DISTURBANCE

One of the main goals of this work is to reduce the unsteady loading on the stator, which arises from the three sources of disturbance as shown in Fig. 1. Results from the *rotor/stator* configuration suggest that the stator response due to vortical disturbance from upstream is much larger than that due to upstream potential disturbance, even for as small an axial gap as 10% chord, and thus can be ignored to first order approximation (Fig. 9). We now proceed to the case of rotor/stator/rotor, using results from rotor/stator and stator/rotor to help interpret the data.

6.1 Effect of Downstream Gap

Figure 14 presents the excursion of the stator suction surface unsteady pressure measured at the 5% chord (Fig. 14a) and 95% chord position (Fig. 14b), for Gap1= 10% chord and Gap2= 10% and 30% chord, at near-design loading. Near the leading edge, Fig. 14a suggests the unsteady pressure is dominated by the upstream rotor, as shown by similarity in the two signatures. Near the trailing edge, Fig. 14b suggests that the unsteady pressure is strongly dependent on the downstream gap spacing, with closer gap produces greater time variation as expected. Note that this variation does not affect the pressure near the leading edge; the exponential decay characteristic of potential disturbance has reached a negligible level at approximately one chord-length upstream.

Figure 15 presents the unsteady force excursion. The force signature shows a large amplitude with the blade-to-blade frequency dominating. Interpretation of this must consider both the effect of upstream vortical and downstream potential disturbances. At this clocking position, 0.7 as shown in Fig. 6a, the force amplitude is twice that of Fig. 9 with only upstream vortical disturbance, and the time occurrence of maximum force, at t/T= 0.3, in Fig. 15b coincides with that of Fig. 9b. These facts suggest that effect of the downstream potential disturbance might be adding to that due to the upstream vortical, thus causing the large amplitude. This proves this to be the case based on the force signature from stator/rotor (Fig. 12) and consideration of rotor clocking. For the rotor/stator/rotor configuration, the instantaneous position of the downstream rotor for clocking = 0.7 at t/T= 0.0 is the same as that at t/T = -0.7, or t/T= 0.3, for stator/rotor (Fig. 6a).

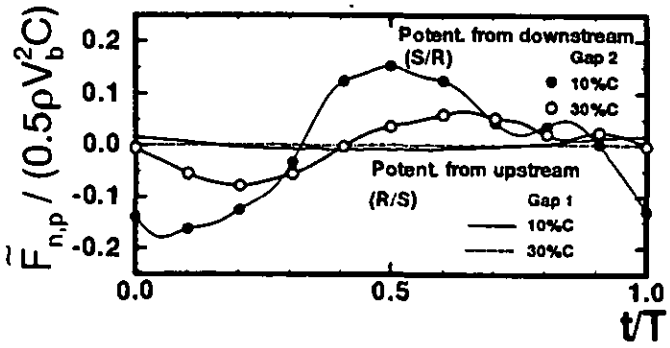

Fig. 13 Potential contributed stator force from upstream (R/S) and downstream (S/R).

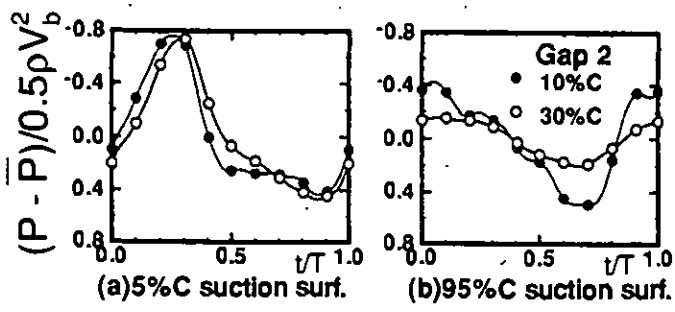

Fig. 14 Unsteady pressure on stator suction surface at 5% and 95% chord, for Gap1= 10% chord and varying Gap2 (clocking = 0.7, R/S/R).

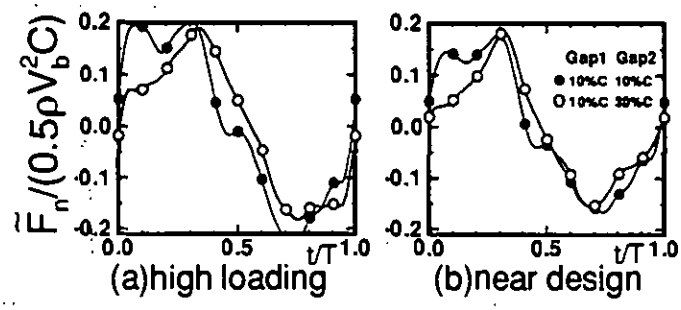

Fig. 15 Unsteady force on stator for Gap1= 10% chord and varying Gap2 (clocking = 0.7, R/S/R).

At non-dimensional time 0.3 later, the rotor/stator/rotor configuration is at t/T= 0.3, when the maximum force occurs, which corresponds to t/T= 0.6 for stator/rotor. At this time, Figs. 12a and 12b show the force is near maximum. Thus contributions due to the upstream vortical and downstream potential disturbances add for clocking = 0.7.

6.2 Effect of Rotor Clocking

We now discuss the effect of clocking the downstream rotor, with respect to the upstream rotor, for rotor/stator/rotor configuration for Gap1= 10% chord and Gap2= 30% chord. Two clocking positions, 0.2 and 0.7, will be presented since they contain major flow phenomena of interest.

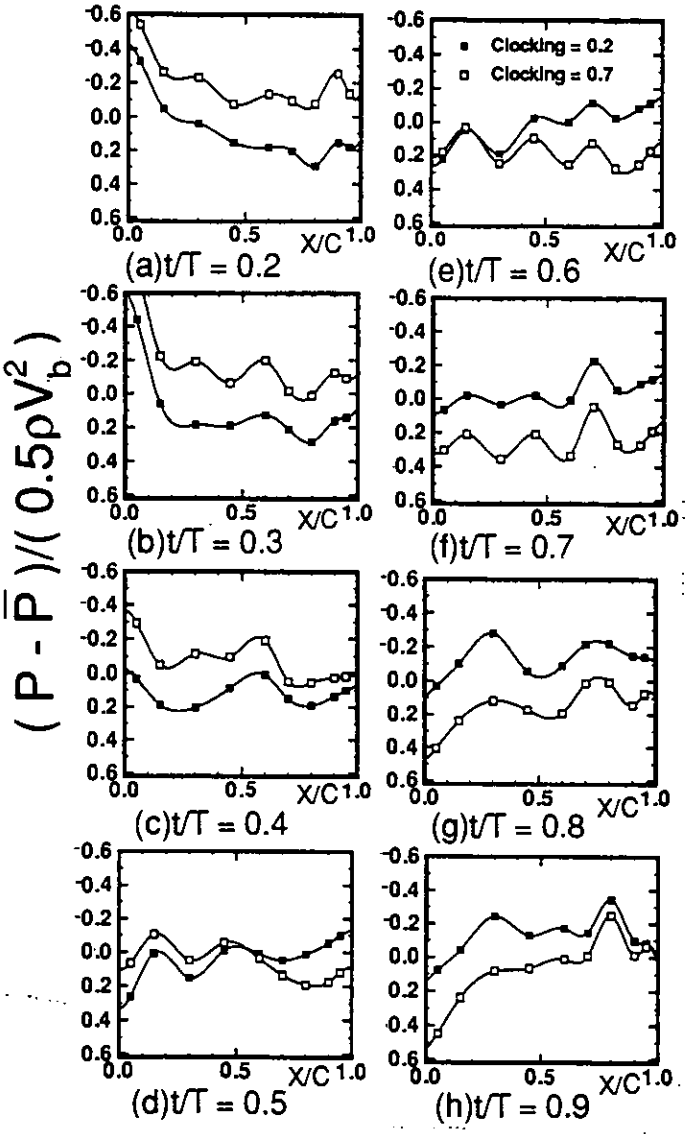

Fig. 16 Unsteady pressure on stator suction surface for clocking = 0.2 and 0.7 (Gap1= 10%C, Gap2= 30%C, R/S/R).

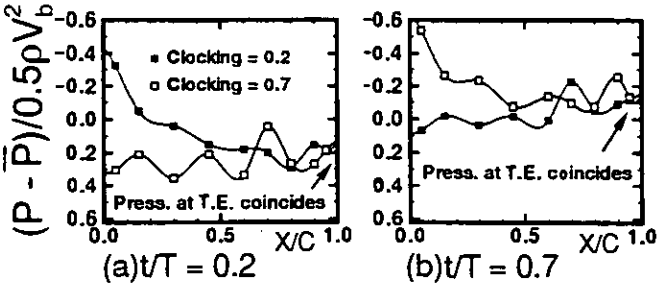

Fig. 17 Unsteady pressure on stator suction surface with clocking = 0.7 data time-shifted by t/T= 0.5 (Gap1= 10%C, Gap2= 30%C, R/S/R).

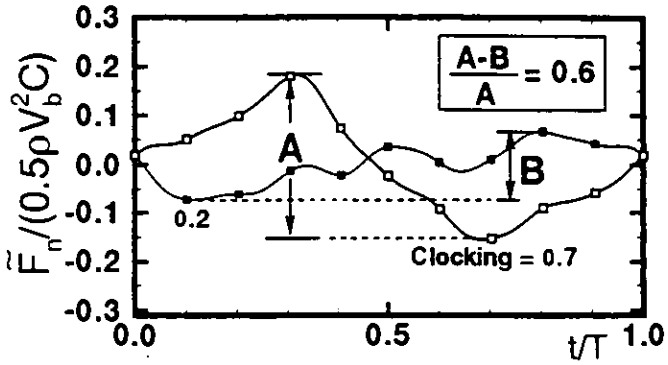

Fig. 18 Unsteady force on stator for clocking = 0.2 and 0.7 (Gap1= 10%C, Gap2= 30%C, R/S/R).

Figure 16 compares the near-design stator suction surface unsteady pressure for both clockings at several time instants. Overall, the chordwise pressure variation of the two curves are similar over the unsteady period, with the major difference in the spatial mean component. Figure 16b shows that both clocking positions have a leading edge suction spike near t/T= 0.3, which is the occurrence of maximum force for rotor/stator configuration (Fig. 9b). The reason for this is that clocking is adjusted for the downstream rotor only; the relative position between the upstream rotor and the stator remains the same for both clocking positions.

Near the trailing edge the unsteady pressure is dominated by the effect of the downstream rotor. Knowing that minimum stator force for stator/rotor configuration occurs at t/T= 0.2, for Gap2= 30% chord (Fig. 12b), this suggests that the trailing edge should have a large positive pressure near t/T= clocking + 0.2, or t/T= 0.4 for clocking = 0.2 and t/T= 0.9 for clocking = 0.7. Figure 16c (t/T= 0.4) for clocking = 0.2 indeed shows that the trailing edge pressure on the suction surface is near maximum before abruptly decreases at t/T= 0.5. Similar trend for clocking = 0.7 is also shown in Fig. 16h (t/T= 0.9), which shows the pressure at the trailing edge already begins to decrease.

Further data interrogation allows one to conclude that the trailing edge pressure is essentially unaffected by the vortical disturbance from upstream. Figure 17 presents results of Fig. 16 at two time instants but with data from clocking = 0.7 case phase-shifted by t/T= 0.5. Physically, the comparison of the two cases - clocking = 0.2 and clocking = 0.7 phase-shifted - implies clocking the *upstream* rotor, with the downstream rotor at the same location for both cases. Figures 17a and 17b, which are representative of all time instants, show that the pressure at the trailing edge is equal for both clocking positions, with a large variation in the pressure near the leading edge.

Figure 18 compares the unsteady force, integrated from Fig. 16, for both clocking positions near design loading. Data show a reduction of 60% in the force amplitude is achieved by clocking the downstream rotor from 0.7 to 0.2 position. Physical reason for the drastic reduction is as follows. Recall that the stator response due to upstream vortical disturbance alone reaches a maximum when the wake impinges against the stator suction surface immediately downstream of the leading edge (Fig. 10), which is near t/T= 0.3 for Gap1= 10% chord (Fig. 9b). Also the stator response due to downstream potential disturbance alone reaches a minimum with a slight time delay after the rotor sweeps pass the stator trailing edge, which is near t/T= 0.2 for Gap3= 30% chord (Fig. 12b). Reduction of the overall stator response is achieved by clocking the downstream rotor so that the time instant when the contribution due to upstream vortical disturbance reaches a maximum coincides with the minimum of that due to downstream potential disturbance. Clocking of 0.2 (see Fig. 6) means the downstream rotor will require t/T= clocking + 0.2= 0.4 to arrive at the same circumferential location, relative to the stator, that will result in minimum stator force for stator/rotor configuration. This t/T= 0.4 is close to the time which maximum force occurs, t/T= 0.3, for stator/rotor configuration, thus contributions to the unsteady force partially cancels. Fine tuning of clocking and axial gap can probably produce further force amplitude decrease, but it is of second order. At high loading, reduction of 56% is achieved with a similar force signature as that at near-design.

6.3 Superposition of Stator Unsteady Loading

With the results for the three configurations it is worthwhile to compare the unsteady response from superposing rotor/stator and stator/rotor configurations with that of rotor/stator/rotor configuration. This is a more strenuous check of the linearity relationship between gust and gust response than that by Giles, in Manwaring and Wisler (1993), using a Navier-Stokes code (UNSFLO). With the inlet boundary condition of a wake/stator calculation based on purely first harmonic (blade-to-blade) gust, measured in the mid-gap of the GE large-scale compressor rig, Giles found that the calculated stator response of the second harmonic was less than 2% of that of the first harmonic. This suggests that non-linearity can be neglected; the gust *response*, even though scales with velocity squared, can indeed be linearized, about a non-linear time-mean (Hall and Crawley, 1989). In the present study, response to gust from upstream *and* downstream of the stator are considered.

The results are presented in Figs. 19 and 20 for clocking = 0.2 and 0.7. Figure 19 shows the stator unsteady force for rotor/stator (Gap1= 10% chord) and stator/rotor (Gap2= 30% chord) configurations with the result of stator/rotor time shifted by t/T= -0.2 and -0.7. The sum of the two curves in each sub-figure can thus be used to compare with that of the rotor/stator/rotor configuration for clocking = 0.2 and 0.7, which is shown in Fig. 20. At near-design loading, good agreement in the *amplitude* is obtained for both clockings (Figs. 20c & 20d). Close examination reveal, however, that for clocking = 0.2 (Fig. 20c) the phase is better matched near the end of the blade-to-blade period than the beginning. This is also seen in Fig. 20d where the phase is slightly off between t/T= 0.7 and 0.9. At high loading, although the agreement in the phase is rather poor for clocking = 0.2 (Fig. 20a) linearity certainly applies for the amplitude. For clocking = 0.7 (Fig. 20b), matching of the amplitude is not as desirable. Overall, data show that linearity is valid with both upstream and downstream gusts, but the agreement for the phase is not as desirable as that for the amplitude.

7.0 FURTHER DISCUSSIONS

7.1 Effect of Clocking on Moment about Mid-chord

Data show clocking of the downstream rotor also reduces the moment about the mid-chord, which is of importance for blade torsional mode. For rotor/stator/rotor configuration with Gap1= 10% chord and Gap2= 30% chord, moment amplitude reduction of 13% is achieved at near-design and 20% at high loading, when the downstream rotor clocking is changed from 0.7 to 0.2 position. The flow physics is essentially identical to that which resulted in force amplitude reduction.

7.2 Different Blade Counts

Results presented herein are for equal count of upstream and downstream rotor blades. If the blade count between successive rotor rows differ then, in a shaft revolution, a stator would experience variation of unsteady amplitude ranging from a minimum, if the rotor rows are optimally clocked at some circumferential location, to a maximum, if the rotor rows are arranged so that the worst clocked position occurs at another circumferential position. The difference between the rotor and stator blade count, however, does not alter results presented, since the disturbances which give rise to stator unsteady load reduction are originated from the upstream and downstream rotors. Hence, the kinematic consideration of interaction tone noise (Tyler and Sofrin, 1962), which is based on the rotor and stator count, is not affected.

8.0 CONCLUSIONS

Experimental study is conducted on rotor/stator, stator/rotor, and rotor/stator/rotor configurations to test a hypothesis – unsteady stator response due to distinct sources of disturbance may partially cancel if their resulted phase relationship can be altered. Sources of disturbances considered are vortical disturbance from the *upstream* rotor, potential disturbance from the *upstream* rotor, and potential disturbance

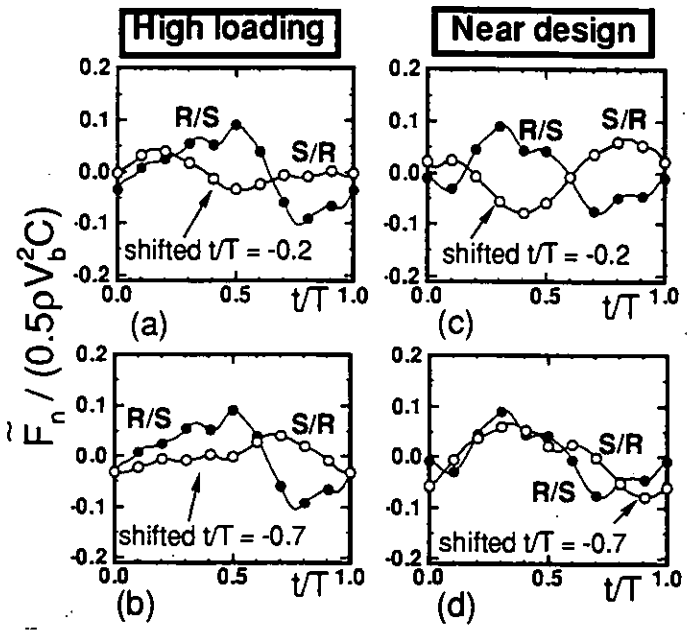

Fig. 19 Unsteady force on stator for rotor/stator and stator/rotor configurations with data from stator/rotor time-shifted (Gap1= 10%C, Gap2= 30%C, R/S, S/R).

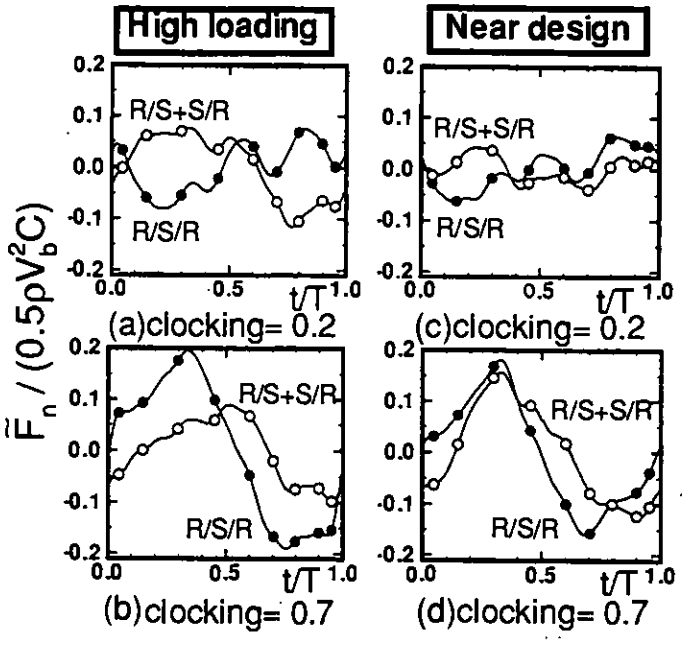

Fig. 20 Comparison of stator unsteady force between the sum of rotor/stator and stator/rotor (time-shifted as in Fig. 19) and that directly from rotor/stator/rotor configuration (Gap1= 10%C, Gap2= 30%C, R/S, S/R, R/S/R).

from the *downstream* rotor. Alteration in the phase relationship of the unsteady sources is achieved by clocking the downstream rotor with respect to the upstream rotor. Major findings are summarized as follow:

- A 60% reduction in the stator unsteady force is found when the clocking of the downstream rotor is changed from 0.7 to 0.2, for rotor/stator/rotor configuration with Gap1= 10% chord and Gap2= 30% chord (Fig. 18).
- In this case, dominant sources of disturbance are vortical disturbance from the upstream rotor and potential disturbance from the downstream rotor, with the upstream potential disturbance negligible (Figs. 9 and 12).
- Stator response due to upstream vortical disturbance reaches a maximum when the wake impinges against the stator suction surface immediately downstream of the leading edge (Fig. 10). This causes a pressure spike near the leading edge region, which is the dominant feature of the unsteady force signature (Fig. 8).
- Stator response due to downstream potential disturbance reaches a minimum with a slight time delay after the rotor sweeps pass the stator trailing edge. The time delay is shown to increase with downstream gap (Fig. 12).
- Physically, reduction of the stator response is achieved by clocking the downstream rotor so that the time instant when the contribution due to upstream vortical disturbance reaches a maximum (Fig. 10) coincides with the minimum of that due to downstream potential disturbance (Fig. 12). (As sketched in Fig. 6b.)
- The unsteady force response contributed by downstream potential disturbance is much larger than that contributed by upstream potential disturbance for the same Gap1 and Gap2. For Gap1=30% chord, the stator response due to upstream disturbance is essentially zero while that due to downstream disturbance is still substantial (Fig. 13).
- Superposing the unsteady response of rotor/stator and stator/rotor configurations and compare with that of rotor/stator/rotor configuration provide a check for the linearity relationship between gust and gust response. Data show that linearity is valid with both upstream and downstream gusts, but the agreement for the phase is not as desirable as that for the amplitude (Fig. 20).

ACKNOWLEDGEMENTS

The authors are grateful for the financial support of the National Science Council, Republic of China (Grant No. NSC 85-2212-E-002-040). The help of Christ throughout the course of this work is also acknowledged.

REFERENCES

Chung, M.H. and Wo, A.M., 1995, "Navier-Stokes and Potential Calculations of Axial Spacing Effect on Vortical and Potential Disturbances and Gust Response in an Axial Compressor," *ASME Paper* 95-GT-301, to appear *J. of Turbomachinery*.

Doebelin, E.O., 1990, Measurement Systems: Application and Design, 4th ed., McGraw-Hill, p. 482.

Feiereisen, J.M., Montgomery, M.D. and Fleeter, S., 1994, "Unsteady aerodynamic forcing functions: a comparison between linear theory and experiment," *ASME paper 93-GT-141.*

Gallus, H.E., Groillus, H., and Lambertz, J., 1982, "The Influence of Blade Number Ratio and Blade Row Spacing on Axial-Flow Compressor Stator Blade Dynamic Load and Stage Sound Pressure Level," *J. Eng. for Power*, Vol. 104, pp. 633-644.

Giles, M.B., 1988, "Calculation of unsteady wake/rotor interaction," *J. of Propulsion and Power*, Vol. 4, pp. 356 - 362.

Goldstein, M.E. and Atassi, H., 1976, "A complete second-order theory for the unsteady flow about an airfoil due to periodic gust," *Journal of Fluid Mechanics*, Vol. 74, part 4: pp. 741-765.

Goldstein, M.E., 1978, "Unsteady vortical and entropic distortions of potential flows round arbitrary obstacles," *Journal of Fluid Mechanics*, Vol. 89, part 3, pp. 433-468.

Hall, K. and Crawley, E., 1989, "Calculation of unsteady flows in turbomachinery using the linearized Euler equations," *AIAA J.*, Vol. 27, No. 6, pp. 777 - 787.

Henderson, G. and Fleeter, S., 1993, "Forcing function effects on unsteady aerodynamic gust response: part 1- forcing functions," *J. of Turbomachinery*, Vol. 115, pp. 741-750.

Henderson, G. and Fleeter, S., 1993, "Forcing function effects on unsteady aerodynamic gust response: part 2 - low solidity airfoil row response," *J. of Turbomachinery*, Vol. 115, pp. 751-761.

Hobbs, D.E. and Weingold, H.D., 1984, "Development of controlled diffusion aerofoils for multistage compressor applications," *J. Eng. for Gas Turbine & Power*, Vol. 106, pp. 271-278.

Hsu, S.T., Wo, A.M. and Wu, C.K., 1996, "Experimental and Numerical Study of Gust and Gust Response in a Rotor/Stator Axial Compressor," presented in the ASME Turbo Asia '96, Jakarta, Indonesian, *ASME Paper 96-TA-043.*

Kerrebrock, J.L., 1992, Aircraft Engines and Gas Turbines, 2nd Ed., M.I.T. Press, p. 371.

Manwaring, S.R. and Wisler, D.C., 1993, "Unsteady aerodynamics and gust response in compressors and turbines," *J. of Turbomachinery*, Vol. 115, pp. 724 - 740.

Tyler, J.M. and Sofrin, T.G., 1962, "Axial Compressor Noise Studies," *SAE Trans.*, Vol. 70, pp. 309-332.

Valkov, T. and Tan, C.S., 1995, "Control of the Unsteady Flow in a Stator Blade Row Interacting with Upstream Moving Wakes," *J. of Turbomachinery*, Vol. 117, pp. 97 - 105.

Weaver, M.M. and Fleeter, S., 1994, "Turbine Rotor Generated Forcing Functions for Flow Induced Vibrations," *ASME paper 94-GT-328.*

Wo, A.M., Chung, M.H. and Hsu, S.T., 1997, "Gust Response Decomposition in a Stator/Rotor Axial Compressor with Varying Axial Gap," *J. of Prop. and Power*, Vol. 13, No. 1.

Appendix Rotor and the stator coordinates*.

ROTOR				STATOR			
RESSURE SUR.		SUCTION SUR.		PRESSURE SUR.		SUCTION SUR.	
X	Y	X	Y	X	Y	X	Y
0.771625	-0.636078	0.000002	0.000001	0.935629	0.352985	0.000000	0.000000
0.772617	-0.632417	0.002822	0.002713	0.934957	0.349194	0.002279	-0.003324
0.767948	-0.62279	-0.005387	-0.0139	0.926439	0.342487	-0.002352	0.01515
0.752036	-0.614321	-0.003911	-0.032516	0.908164	0.341587	0.003056	0.033618
0.730906	-0.603092	0.002765	-0.05642	0.883908	0.340367	0.014603	0.05643
0.705539	-0.589495	0.014023	-0.084083	0.85474	0.338756	0.031501	0.082143
0.676918	-0.57396	0.029048	-0.114357	0.821749	0.336703	0.052784	0.109699
0.645953	-0.556872	0.047388	-0.146153	0.785944	0.334135	0.077857	0.138006
0.613433	-0.538549	0.068511	-0.178633	0.74819	0.330969	0.106066	0.166241
0.580003	-0.519215	0.091902	-0.211182	0.709185	0.327094	0.136772	0.193848
0.546167	-0.499024	0.117224	-0.243297	0.66947	0.322385	0.169637	0.22021
0.512256	-0.478136	0.144291	-0.274543	0.629428	0.316823	0.20434	0.244892
0.478498	-0.456642	0.173162	-0.304405	0.589321	0.310393	0.24088	0.267152
0.445124	-0.434469	0.203577	-0.332769	0.549362	0.302834	0.278937	0.286824
0.412295	-0.411533	0.235407	-0.359501	0.509695	0.293957	0.318323	0.303619
0.380116	-0.387758	0.268475	-0.384624	0.470439	0.283565	0.358783	0.317513
0.348665	-0.363072	0.302523	-0.408353	0.43169	0.271514	0.399984	0.328921
0.318023	-0.33739	0.337289	-0.43102	0.393562	0.257627	0.441692	0.338324
0.288336	-0.31057	0.372648	-0.452803	0.356272	0.24156	0.483764	0.346092
0.259666	-0.282609	0.408578	-0.473713	0.320002	0.223223	0.526143	0.352267
0.232251	-0.253391	0.444944	-0.493898	0.285078	0.202392	0.568714	0.357129
0.2058	-0.223361	0.481672	-0.513305	0.251265	0.179889	0.611358	0.360711
0.180127	-0.192912	0.518541	-0.532014	0.218534	0.156165	0.653873	0.363265
0.155353	-0.162272	0.555252	-0.550044	0.186988	0.131585	0.695974	0.364997
0.131616	-0.131811	0.59147	-0.567225	0.156781	0.106608	0.737261	0.365897
0.108639	-0.102392	0.626661	-0.583439	0.127727	0.082291	0.777177	0.366135
0.086626	-0.074713	0.660135	-0.59851	0.100222	0.059224	0.814997	0.365898
0.065858	-0.04963	0.691052	-0.612182	0.07466	0.038268	0.849818	0.365352
0.046692	-0.028162	0.718436	-0.624127	0.051545	0.020409	0.880588	0.364654
0.029294	-0.011755	0.741235	-0.633982	0.031249	0.007093	0.906167	0.363954
0.014248	-0.001884	0.758432	-0.641359	0.014556	-0.000331	0.925437	0.363372
0.003611	0.001112	0.769291	-0.639247	0.003425	-0.001711	0.93481	0.356954
0.000002	0.000001	0.771625	-0.636078	0.000000	0.000000	0.935629	0.352985

* For code validation contact the second author (E-mail address on the first page) if you need the coordinates in a file or other additional information.